Journal of Biomolecular NMR, **21:** 107–116, 2001.
KLUWER/ESCOM

Simultaneous measurement of intra- and intermolecular NOEs in differentially labeled protein-ligand complexes*

Christian Eichmüller, Wolfgang Schüler, Robert Konrat** & Bernhard Kräutler
Institute of Organic Chemistry, University of Innsbruck, Innrain 52a, A-6020, Innsbruck, Austria

Received 15 May 2001; Accepted 26 July 2001

Key words: drug design, enzyme-ligand complexes, NOESY, protein NMR spectroscopy, protein-protein complexes, SAR by NMR

Abstract

A new NOE strategy is presented that allows the simultaneous observation of intermolecular and intramolecular NOEs between an unlabeled ligand and a ^{13}C,^{15}N-labeled protein. The method uses an adiabatic ^{13}C inversion pulse optimized to an empirically observed relationship between $^{1}J_{CH}$ and carbon chemical shift to selectively invert the protein protons (attached to ^{13}C). Two NOESY data sets are recorded where the intermolecular and intramolecular NOESY cross peaks have either equal or opposite signs, respectively. Addition and subtraction yield two NOESY spectra which contain either NOEs within the labeled protein (or unlabeled ligand) or along the binding interface. The method is demonstrated with an application to the B_{12}-binding subunit of Glutamate Mutase from *Clostridium tetanomorphum* complexed with the B_{12}-nucleotide loop moiety of the natural cofactor adenosylcobalamin (Coenzyme B_{12}).

Introduction

NMR spectroscopy has become a powerful tool to study biologically important noncovalent assemblies of macromolecules in solution and yielded a wealth of information on the structural details of molecular recognition (Clore and Gronenborn, 1997). The most efficient experimental strategy relies on uniform labeling of one of the components with ^{15}N and/or ^{13}C, while leaving the second component unlabeled (Otting et al., 1986; Otting and Wüthrich, 1990; Sattler et al., 1999; Breeze, 2000). This approach allows the selection of intermolecular NOEs between the two constituents of the macromolecular complex (Wider et al., 1990, 1991; Folkers et al., 1993, 1994; Bax et al., 1994; Yang et al., 1995). The accuracy and precision of the complex structure is particularly sensitive to the number of intermolecular NOE connectivities, thus making the NOE assignment the essential (and time consuming) part of the structure elucidation process (Clore, 2000). Specifically, the editing/filtering NMR experiments devised for this purpose employ the one-bond heteronuclear scalar couplings to select for/against protons that are bound at sites carrying an isotope label. A major hurdle to a general application of the method is due to variations in JCH scalar coupling constants (between 120–220 Hz). This problem has been overcome (in part) by developing second-(high)-order isotope filters (Gemmecker et al., 1992; Ikura and Bax, 1992; Lee et al., 1994; Dalvit et al., 1998; 1999; Sattler et al., 1999; Breeze, 2000), in particular by means of adiabatic inversion pulses with a sweep rate adjusted to an empirical J_{CH} vs ^{13}C chemical shift profile (Zwahlen et al., 1997) or based on a J-compensated isotope filter through isomorphism to composite pulse rotations (Stuart et al., 1999). The drawback of loosing all intramolecular NOEs of the labeled macromolecule was recently overcome by a J-spectroscopy based 4D experiment for simultaneous recording of inter- and intramolecular NOEs (Melacini, 2000).

*This paper is dedicated to Prof Peter Schuster on the occasion of his 60th birthday.

**To whom correspondence should be addressed. E-mail: robert.konrat@uibk.ac.at

Here we report a filtering/editing technique based on selective inversion of protons bound to ^{13}C (using adiabatic pulses with optimized sweep rates) and ^{15}N, and with subsequent addition and subtraction of the 3D NOESY data sets to simultaneously identify intra- and intermolecular NOE connectivities. The filtering strategy is related to the 'linear-combination'-type filters filters and edits introduced by Wüthrich and coworkers (Wörgötter et al., 1986; Otting et al., 1986; Otting and Wüthrich, 1990). The proposed sequence provides good NOE selectivity and offers an improvement in sensitivity for the measurement of intramolecular NOEs relative to the previously devised semi-constant J-resolved 4D experiment (Melacini, 2000). The method is applied to the B_{12}-binding subunit of Glutamate Mutase from *Clostridium tetanomorphum* complexed with the B_{12}-nucleotide loop moiety of the natural cofactor Coenzyme B_{12}.

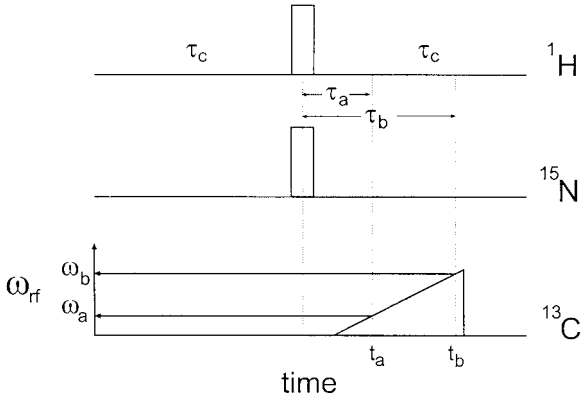

Figure 1. J-coupling evolution scheme for selective inversion of protons that are scalar coupled to ^{15}N or ^{13}C spins. The rf carrier frequency of the ^{13}C inversion pulse is modified. Carbon magnetizations of carbons resonating at ω_a and ω_b are inverted at different times t_a and t_b. The rate of the frequency sweep ($d\omega/dt$) is optimized with respect to the $^1J_{CH}$ vs δ_C relationship. $2\tau_c = 1/J_{NH}$, so that protons bound to ^{15}N will be inverted. The net evolution time during which the heteronuclear J_{CH} scalar coupling evolves is $2\tau_c - 2\tau_a$ (for carbon spin with resonance frequency ω_a) or $2\tau_c - 2\tau_b$ (for carbon spin with resonance frequency ω_b).

Materials and methods

All NMR experiments were performed on a Varian UNITYPlus 500 MHz spectrometer equipped with a pulse field gradient unit and triple resonance probes with actively shielded z gradients. All spectra were recorded at 26 °C. ^{13}C,^{15}N-labeled MutS was overexpressed in *E. coli* and purified as described previously (Hoffmann et al., 2001). The NMR sample contained 2.0 mM ^{13}C,^{15}N-labeled MutS, 5 mM DTT, 1 mM EDTA, 0.03% NaN_3, and 10 mM phosphate buffer at pH 6.9, dissolved in 90%H_2O/10%D_2O. In the binary complex, the ^{13}C,^{15}N MutS:B_{12}-nucleotide ratio was 1.0:12.0. The B_{12}-nucleotide was prepared as described elsewhere (Eschenmoser, 1988; Bartels et al., 1991). The dissociation constant of the complex K_d was determined from a titration of the protein with the B_{12}-nucleotide by a non-linear least squares fitting of the chemical shift changes as a function of ligand concentration ($K_d = 5.6 \pm 0.7$ mM; Tollinger et al., 2001). The 3D SIM-NOESY-HSQC was recorded with the pulse scheme of Figure 3 (180 ms NOESY mixing time). Intra- and intermolecular NOESY spectra were obtained by post-acquisition addition and subtraction of the data (recorded in an interleaved manner). A data matrix consisting of 45, 35 and 512 complex points in each of t_1, t_2 and t_3 was acquired, the following spectral windows were used: F1: 6000 Hz, F2: 3000 Hz and F3: 8000 Hz. A relaxation delay of 1 s was used along with 16 scans per FID. For comparison a 150 ms 3D ^{13}C,^{15}N NOESY-HSQC (Pascal et al., 1994) was recorded. A data matrix consisting of 45, 50 and 512 complex points in each of t_1, t_2 and t_3 was acquired, the following spectral windows were used: F1: 6000 Hz, F2: 3000 Hz and F3: 8000 Hz. Again, a relaxation delay of 1 s and 16 scans were used. All spectra were processed identically using NMRPipe/NMRDraw software (Delaglio et al., 1995) and analyzed using the program NMRView (Johnson and Blevins, 1994). The sizes of the two 3D HSQC-NOESY data set were doubled in both indirect frequency dimensions and the data set were apodized in each dimensions with a squared sine-bell window function, zero filled, Fourier transformed, phased, and the imaginaries eliminated. The final data set comprised $256 \times 128 \times 512$ real points.

Figure 1 illustrates the basic element which is used to selectively invert the protons bound to ^{13}C or ^{15}N. The overall delay $2\tau_c$ is set to $2\tau_c = 1/J_{NH}$, so that protons bound to ^{15}N will be inverted. Due to the dependence of J_{CH} on ^{13}C chemical shift a different strategy is employed for inversion of protons bound to ^{13}C. The effect of an adiabatic inversion pulse can be appreciated by considering that spin inversion occurs when the frequency sweep passes through the resonance frequency of the carbon of interest, provided that the overall sweep width is large compared to the radio-frequency (rf) field. We consider two carbons with their resonance frequencies ω_a and ω_b, respectively. If we start the frequency sweep from the

up-field side of the spectrum, the accelerating reference (spin-lock) frame will pass through the resonance frequency ω_a at time point t_a, whereas the frequency ω_b will be matched at a later time t_b. Thus the time when the two carbons are inverted will be different, resulting in a different net evolution time during which the heteronuclear JCH scalar coupling evolves ($2\tau_c - 2\tau_a$ or $2\tau_c - 2\tau_b$). A substantial improvement in ^{1}H inversion efficiency can be achieved by adjusting the sweep rate of the adiabatic pulse to the almost linear relation between the one bond ^{1}H-^{13}C scalar coupling, J_{CH}, and carbon chemical shift, δ_C, ($J_{CH} = A\delta_C + B$, where $A = 0.71$ Hz/ppm; $B = 101$ Hz) (Zwahlen et al., 1997). Figure 2B shows the improvement obtained by J_{CH} compensation using the scheme of Figure 1 compared to a conventional INEPT-type echo sequence (Figure 2A) with $2\tau_c = 1/J_{CH}$. Although the linear J_{CH} vs ^{13}C chemical shift profile can be best accomplished by a hyperbolic $\omega_{rf}(t)$ profile, we used optimized linear frequency sweeps as described elsewhere (Zwahlen et al., 1997). The outcome of the basic sequence element of Figure 1 was determined from density matrix calculations assuming a heteronuclear two-spin system. In all calculations a total sweep width of 60 kHz and adiabatic pulse durations of 2.8 ms (γB_1: 5.0 kHz) were employed.

The 3D SIM-NOESY-HSQC experiment for simultaneous measurement of inter- and intramolecular NOEs is outlined in Figure 3. In terms of the flow of magnetization it is analogous to the ^{13}C,^{15}N-edited NOESY-HSQC experiment of Kay and co-workers (Pascal et al., 1994), however, preceded by the pulse sequence element of Figure 1. Two data sets are recorded where in one experiment the heteronuclear ^{13}C and ^{15}N inversion pulses are omitted and the one-bond $^1J_{CH}$ and $^1J_{NH}$ scalar couplings are refocused. The 90° ^{1}H radio-frequency (rf) pulse (before the NOESY period τ_m) returns both ligand and protein ^{1}H transverse magnetizations to the z-axis. In contrast, in the second experiment the pulse scheme of Figure 1 is applied and both $^1J_{CH}$ and $^1J_{NH}$ couplings are active during the time $2\tau_C$ (see above). In this case (after the 90° ^{1}H pulse), the ligand and protein proton Zeeman reservoirs are aligned in an anti-parallel manner. Thus, the sign of the intermolecular NOESY cross peaks is inverted, whereas the intramolecular NOEs (within the ligand and the protein) are unchanged. Addition and subtraction give separate data sets for intra- and intermolecular NOEs, respectively. The two data sets were recorded in an interleaved manner and added and subtracted afterwards.

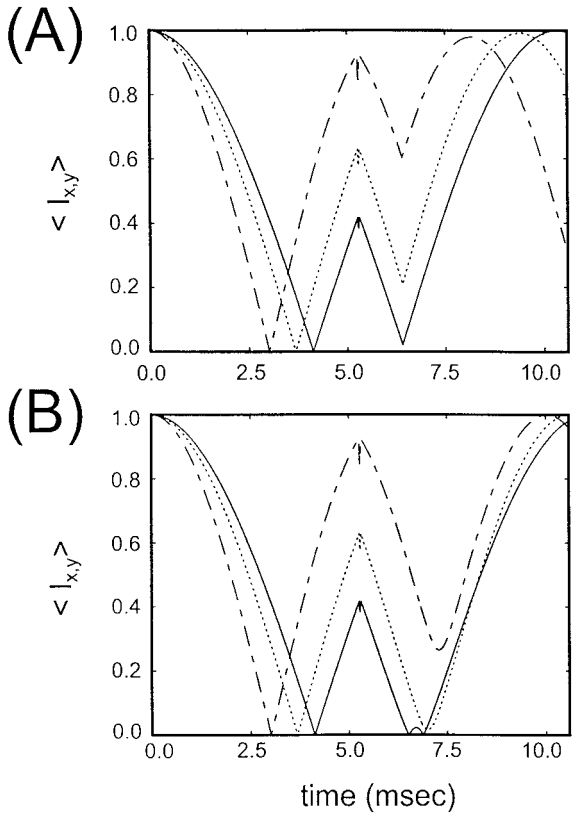

Figure 2. Simulation of the time evolution of the expectation values for transverse ^{1}H magnetization $\langle I_{x,y'} \rangle$ during a ^{1}H-^{13}C INEPT sequence. (A) Application of a hard ^{13}C 180° pulse (5 μs) optimized for a J_{CH} coupling of 120 Hz (applied at 6.35 ms). (B) Adiabatic inversion pulse (sweep width: 60 kHz; pulse duration: 2.8 ms; γB_1: 5.0 kHz; apodization of the first and last 30% using a sine function). The hard ^{1}H rf pulse (5 μs) was applied in the middle of the INEPT step (after 5.26 ms). The magnitude, $I_{x,y} = (I_x^2 + I_y^2)1/2$, of in-phase ^{1}H magnetization is shown. Simulations for three different J_{CH} values are shown: 120 Hz (solid); 140 Hz (dotted); 169 Hz (dashed-dotted).

Results and discussion

The proposed sequence (Figure 3) was applied to the B_{12}-binding subunit of glutamate mutase (MutS) from *Clostridium tetanomorphum* in complex with the nucleotide portion of the natural cofactor coenzyme B_{12}. The solution structure of MutS has recently been published (Tollinger et al., 1998; Hoffmann et al., 2001) and revealed that the global fold of MutS in solution is similar to the crystal structures of other B_{12}-binding domains (Drennan et al., 1994; Mancia et al., 1996; Reitzer et al., 1999). The MutS/B_{12}-nucleotide has recently been investigated using a ^{15}N-labeled MutS sample, the dissociation constant K_d of the complex

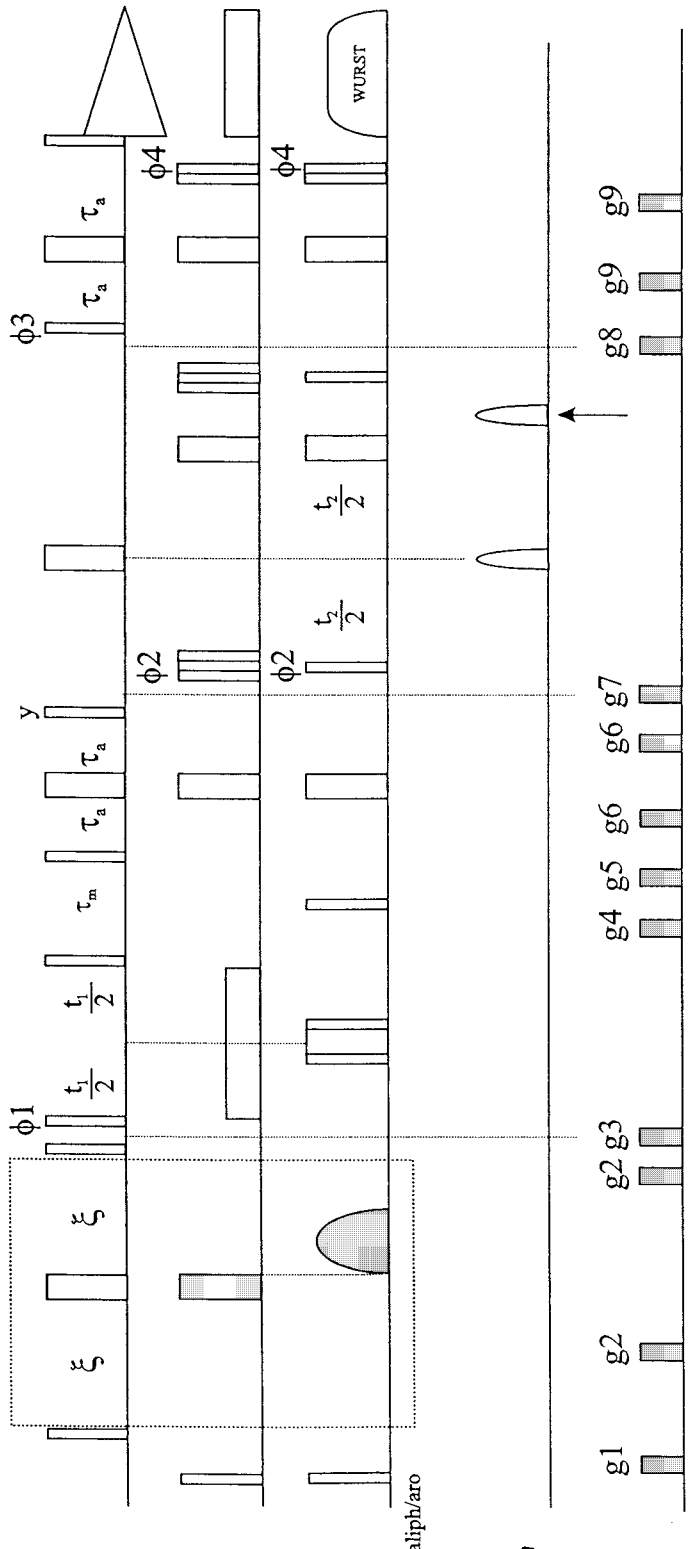

Figure 3. Pulse scheme for simultaneous recording of intra- and intermolecular NOEs in protein-ligand complexes based on differential relaxation of longitudinal ^{1}H magnetization induced by selective ^{1}H inversion of protons attached to the ^{13}C,^{15}N-labeled proteins. Experimental scheme to establish the difference mode (Δ anti-parallel alignment of ^{13}C,^{15}N-protein and ligand ^{1}H magnetizations). The experiment for the generation of the sum mode (Σ, parallel alignment of ^{13}C,^{15}N-protein and ligand ^{1}H magnetizations) is obtained by omitting the ^{15}N and the adiabatic ^{13}C rf pulses in the boxed region (shown in grey). Narrow and wide pulses indicate 90° and 180° pulses, respectively, and, unless indicated otherwise, all pulses are applied along the *x*-axis. Broadband ^{13}C inversion (during ξ) is achieved using a WURST adiabatic pulse (Kupce and Freeman, 1995) with a peak $\gamma B_1 = 4.5$ kHz and with apodization of the first and last 30% using a sine function (Böhlen and Bodenhausen, 1993), a 60 kHz frequency sweep, and a duration of 2.8 ms. All rectangular ^{1}H and ^{13}C hard pulses (applied to $^{13}C_{aliph/aro}$) are applied with 28 and 20 kHz, respectively. ^{15}N decoupling during t_1 is achieved with use of a WALTZ-16 field (^{15}N $\gamma B_1 = 840$ Hz) (Shaka et al., 1983). The ^{13}C' shaped pulses have SEDUCE (McCoy and Müller, 1992) profiles (240 µs, 4.55 kHz peak rf). The arrow indicates the position of the ^{13}C' shaped pulse necessary for Bloch-Siegert compensation. The composite ^{15}N 90° rf pulses (before and after t_2) are applied to ensure a first-order phase correction of 180° (Pascal et al., 1994). ^{13}C and ^{15}N decoupling during acquisition were achieved with WURST (Kupce and Freeman, 1995) ($\gamma B_1 = 3.0$ kHz) and GARP (Shaka et al., 1985) ($\gamma B_1 = 840$ Hz) decoupling scheme. The values for ξ and τ_a, were set to 5.26 and 1.7, respectively, and the NOESY mixing time τ_m was set to 180 ms. Gradient levels were as follows: g1=1.0 ms, 15 Gcm^{-1}; g2=1.0 ms, 8 Gcm^{-1}; g3=0.3 ms, 4 Gcm^{-1}; g4=1.0 ms, 15 Gcm^{-1}; g5=1.0 ms, 20 Gcm^{-1}; g6=1.0 ms, 8 Gcm^{-1}; g7=4.0 ms, 19 Gcm^{-1}; g8=3.0 ms, −18.8 Gcm^{-1}, and g9=1.0 ms, 8 Gcm^{-1}. The phase cycling was $\phi1 = 4(x), 4(-x)$; $\phi2 = 8(x), 8(-x)$; $\phi3 = (x, y, -x, -y)$; $\phi4 = 4(x), 4(-x)$ and receiver was $(x, -y, -x, y), 2(-x, y, x, -y), (x, -y, -x, y)$. Quadrature detection in F_1 and F_2 is achieved by States-TPPI (Marion et al., 1989) of $\phi1$ and $\phi2$.

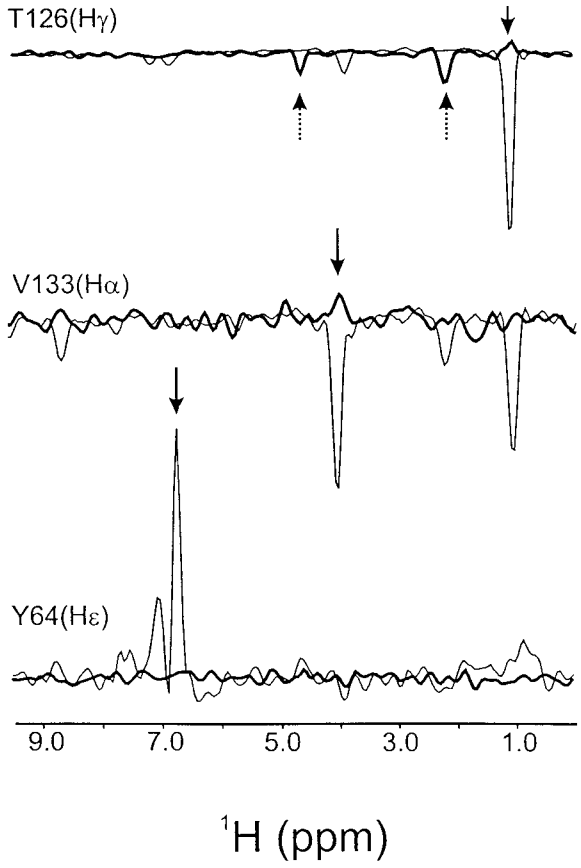

Figure 4. Illustration of the $^1J_{CH}$ compensation obtained with the pulse sequence element of Figure 1. 1D traces through F1 of the 3D ^{13}C,^{15}N SIM-NOESY-HSQC (Figure 3). NOESY mixing time τ_m was set to 180 ms. 1D traces showing the protein proton magnetizations (addition of the two data sets, intramolecular NOE data set) attached to carbon nuclei in the methyl (T126), Cα aliphatic (V133) and ^{13}C aromatic (Y64) region of the^{13}C spectral range (thin line). Residual protein proton magnetization (subtraction of the two data sets, intermolecular NOE data set) (thick line). The ^{13}C chemical shifts of the selected carbons are as follows: T126(Cγ:22.6 ppm), V133(Cα:64.2 ppm) and Y64(Cε:118.4ppm). Solid arrows indicate the diagonal peaks, dashed arrow indicate intermolecular NOEs, T126(Hγ)-H(C10/C11), see also Figure 6B, and NOEs to bulk water, respectively.

was determined to 5.6 ± 0.7 mM (Tollinger et al., 2001).

Experimental verification of the purging efficiency of the inversion element (Figure 1) is presented in Figure 4. 1D traces of selected carbons taken along the diagonal peaks of the intramolecular protein-protein (addition of the two data set) and corresponding traces from the intermolecular protein-ligand (subtraction of the two data set) NOESY map obtained with the sequence of Figure 3 are shown. Substantial suppression of protein diagonal peaks in the intermolecular NOESY is achieved throughout the entire carbon spectrum (CH_3(T126Hγ): 4.8%; Cα(V133Hα): 8.4% and C_{arom}(Y64Hε): 4.2%). The experimental suppression levels are in qualitative agreement with the values calculated in Figure 2B. Most importantly, the trace of T126Hγ (Figure 4A), shows that both good suppression of protein ^{1}H signals and still intense intermolecular NOE cross-peaks are obtained with this experimental scheme. Although slightly better suppression levels might be achieved by employing more sophisticated (hyperbolic) frequency sweeps, for the sake of ease of implementation we suggest using linear sweeps.

The performance of the sequence was further validated by inspection of intramolecular NOEs between protons of ^{13}C,^{15}N-labeled protein (Figure 5). For comparison we recorded a conventional 3D ^{13}C,^{15}N-NOESY-HSQC (Figures 5a, 5c, and 5e) (Pascal et al., 1994). Representative expansions from the (F1,F3) NOE planes extracted at carbon frequencies typical for ^{13}Cα (F2 = 64.2 and 56.5 ppm) and ^{13}C methyl groups (F2 = 21.8 ppm) are shown (Figure 5). In both data sets essentially the same NOE connectivities were observed, indicating that the sequence can be used for recording intramolecular NOEs on the same protein sample under identical experimental conditions. The slight differential increase and decrease of NOE connectivities in panels e and f may be due to indirect water mediated dipolar relaxation pathways. In addition, the proposed sequence offers the possibility to discriminate between intermolecular NOEs to bound water molecules and intramolecular NOEs to Hα's with chemical shifts close to the water resonance frequency. It is noteworthy to compare our approach in terms of sensitivity with the previously proposed 4D *J*-resolved experiment (Melacini, 2000). In the *J*-resolved spectrum the signal intensity is reduced by a factor of 2 because the ^{13}C-bound ^{1}H spins appear at $\pm^1J_{CH}/2$ in the indirect frequency dimension and since the intramolecular NOESY spectrum is obtained by extracting the various NOE planes from the 4D data set at F2 = $^1J_{CH}/2$. The necessary spectral resolution (e.g. to resolve the ^{13}C-^{1}H doublet) along the J-dimension is achieved by adopting a constant-time (CT) version of the *J*-resolved experiment, which leads to an additional reduction due to ^{1}H transverse relaxation (Melacini, 2000). The overall length of the CT-J block in the *J*-resolved experiment was about 11.3 ms compared to 2ξ = 10.52 ms (Figure 3) in our case. A second important consideration is that the $^1J_{CH}$ scalar couplings are not uniform and thus an op-

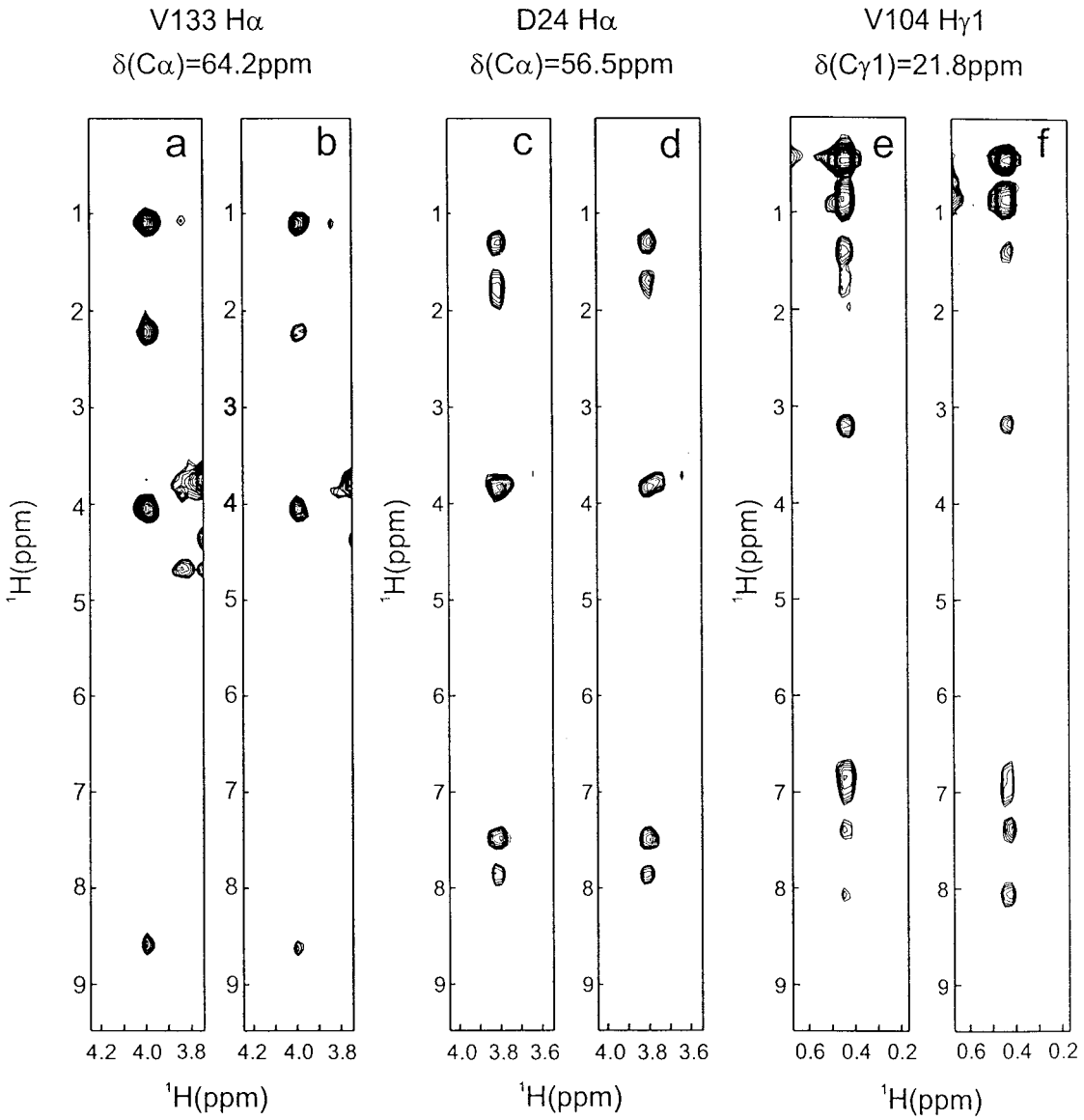

Figure 5. Identification of intramolecular protein NOEs. Representative plots from the (F_1,F_3) NOE plane extracted from the 3D experiment of Figure 3 (τ_m = 180 ms) after addition of the data set. ^{13}C spectral regions for methyl group (21.8 ppm) and two selected Cα regions (56.5 and 64.2 ppm) are shown. For comparison conventional ^{13}C,^{15}N NOESY-HSQC spectra (Pascal et al., 1994) (τ_m = 150 ms) are also given. (a), (c) and (e) ^{13}C,^{15}N NOESY-HSQC; (b), (d) and (f) intramolecular subset of ^{13}C,^{15}N SIM-NOESY-HSQC (Figure 3). Acquisition and processing parameters are given in Materials and methods.

timal F2 selection cannot be simultaneously achieved for all ^{13}C bound protein protons.

An illustration of the observation of intermolecular NOEs is illustrated in Figure 6, where sections from the 3D SIM-NOESY-HSQC (τ_m = 180 ms) are shown. The data sets were recorded on an unlabeled B_{12}-nucleotide-loop/^{13}C,^{15}N-MutS complex using the sequence of Figure 3 and by subtracting the two 3-dimensional FIDs (sum and difference of protein and ligand proton Zeeman reservoirs during τ_m). Figure 6B shows three (^{13}C,^{1}H) planes extracted at the ^{1}H chemical shifts (F1) of R5, Pr3 and C10/C11. the protons C10 and C11 are isochronous and cannot be distinguished. In Figure 6B correlations connecting the protons R5 on the B_{12}-nucleotide loop, with I22δ1, I22γ2 and V18γ2 on MutS are observed. Additionally, NOEs between Pr3 and I22δ1, V18γ1 and V18γ2, as well as between C10/C11 and T121γ,

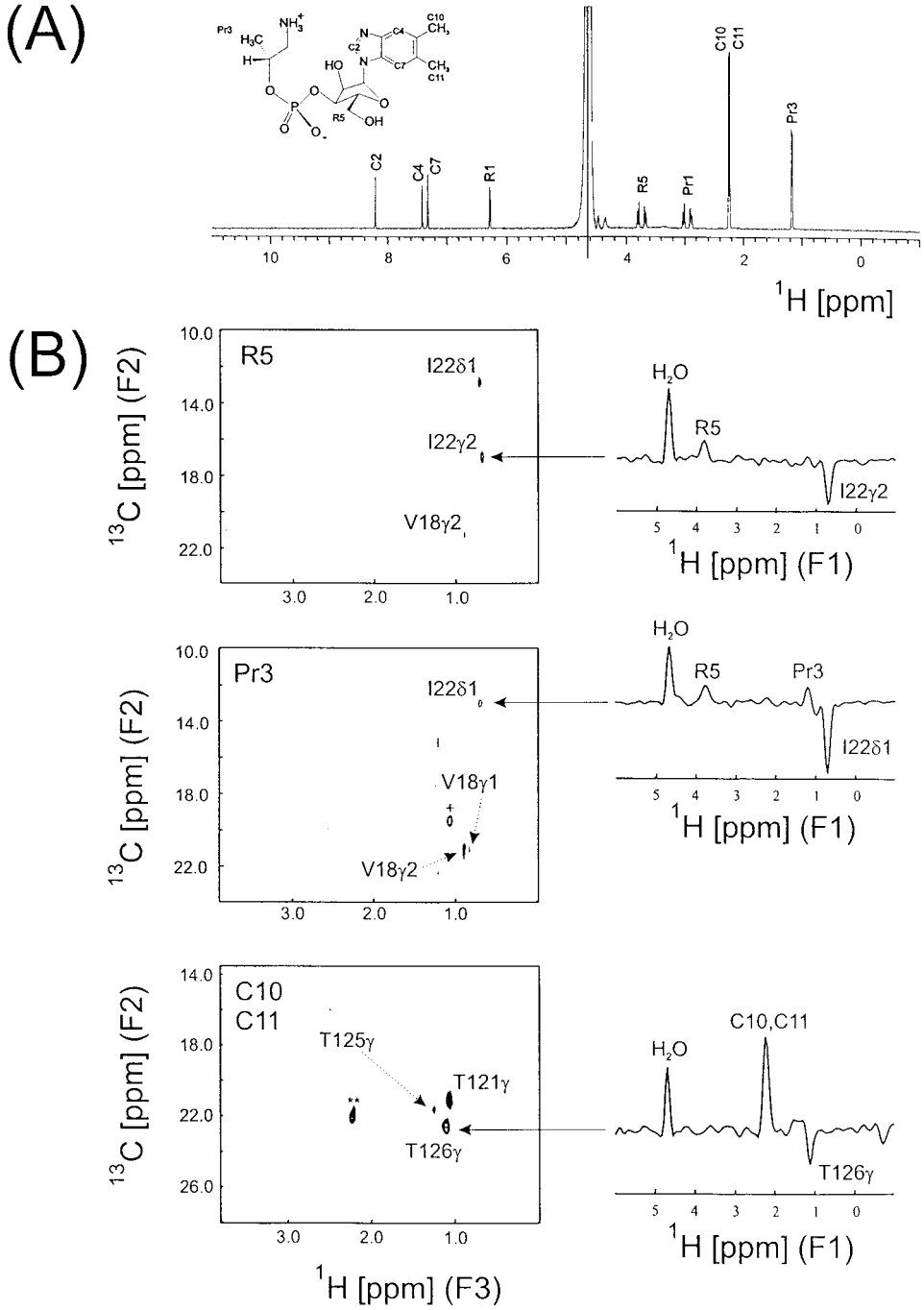

Figure 6. (A) Molecular formula, numbering scheme and 1D spectrum of the nucleotide loop. (B) Selected (F_2,F_3) planes from the 3D ^{13}C,^{15}N SIM-NOESY-HSQC (τ_m = 180 ms) of unlabeled B_{12}-nucleotide loop/^{13}C,^{15}N-labeled MutS recorded with the sequence of Figure 3. Ligand signals are observed along F_1, while protein signals are observed in F_2 (^{13}C) and F_3 (^{1}H). (^{13}C,^{1}H) planes are taken at the ^{1}H F_1-frequency of the indicated protons (R5, Pr3, and C10/C11) of the nucleotide loop. In the middle panel (Pr3) of Figure 6B, the correlation peak marked with + has increased intensity in the adjacent slice and is due to a low molecular weight impurity. The intramolecular ligand cross-peak at natural ^{13}C abundance between the degenerate methyl groups C10 and C11 is indicated by ** (lower panel, Figure 6B, C10,C11). Improved filtering of unwanted intramolecular protein signals in the intermolecular 3D NOESY-HSQC data set is demonstrated by F_1 traces taken at the corresponding F_2 (^{13}C) and F_3 (^{1}H) frequencies of residues I22γ2, I22δ1 and T126γ (indicated by arrows). Intermolecular and (remaining unwanted) intramolecular NOEs appear as positive and negative peaks, respectively, and are labeled either above (ligand) or below (protein) the horizontal traces.

T125γ and T126γ are found. The efficacy of the filtering scheme is additionally demonstrated in Figure 6B where traces for residues I22γ2, I22δ1 and T126γ along the F1 frequency dimension of the intermolecular 3D NOESY-HSQC data set are shown. Although only weak NOEs are detected in this low-affinity complex (K_d = 5.6 mM, Tollinger et al., 2001), the suppression of intramolecular protein NOESY peaks is sufficient to ensure the unambiguous assignment of intermolecular NOEs. Additionally, note that remaining intramolecular diagonal peaks of the $^{13}C,^{15}N$-labeled protein are of opposite sign (with respect to the intermolecular cross peaks), whereas remaining intramolecular diagonal peaks of the ligand (at natural ^{13}C abundance) are of the same sign. All of the observed intermolecular NOEs could be unambiguously assigned based on the ^{15}N solution structure of the B_{12}-nucleotide-loop/MutS complex (Tollinger et al., 2001). The only exception, however, were weak NOEs observed between an (unassigned) aliphatic ^{13}C-^{1}H spin system (^{1}H: 2.39; ^{13}C: 33.6 ppm) and methyl protons of I47, L74, I86, and L88. Interestingly, these side-chains form a hydrophobic cluster in the 3D structures of the apo-form of MutS (Hoffmann et al., 2001) and also in the MutS complex (Tollinger et al., 2001). The side-chains of these residues are adjacent to both a buried arginine side-chain (R75) and the thiol group of C78. We think that these NOEs are due to subtle changes in the intramolecular relaxation pathways of the protein protons mediated by exchangeable hydroxyl protons and/or internally bound water molecules which slightly alter the NOE cross peak intensities in the two experiments (sum or difference mode). We are currently investigating experimental possibilities to suppress these indirect relaxation pathways (e.g., suitable water inversion pulses in the middle of the NOESY mixing time applied according to the QUIET-NOESY technique, Zwahlen et al., 1994), as well as to possibly exploit this effect for hydration studies of proteins. It is important to note that the sequence of Figure 3 allows to record both intra- and intermolecular NOEs involving ^{15}N bound amide protons. Specifically, the following intermolecular NOEs were observed: C10/C11-$^{1}H^{N}$(V90, G91, G92, Y117, T121, T126); C4-(V60, G91, G92); R5-(D24). Similar NOE connectivities were obtained on the ^{15}N-labeled sample (Tollinger et al., 2001).

The utility of the observed intermolecular NOEs obtained with the new sequence for structure determination of the MutS/B_{12}-nucleotide loop complex is illustrated in Figure 7. In Figure 7A the X-ray structure of the homologous protein glutamate mutase from *clostridium cochlearium* is shown together with the nucleotide moiety of the bound methylcobalamin (Reitzer et al., 1999). Figure 7B indicates the observed intermolecular NOEs obtained with the sequence of Figure 3. Sequence comparison between the B_{12}-binding subunit of glutamate mutase from *Clostridium cochlearium* (GlmS) and MutS revealed that residues V125 and G126 in GlmS are replaced by T125 and T126. The structure used in Figure 7B was thus modelled accordingly. These NOEs provide critical restraints for establishing the correct binding mode of the nucleotide loop of the coenzyme to the B_{12}-binding subunit of glutamate mutase, MutS. As we have discussed in some detail previously (Tollinger et al., 2001), ^{15}N chemical shift perturbation and intermolecular NOEs (obtained from a ^{15}N-labeled protein sample) indicate a similar binding location of the B_{12}-nucleotide loop in the MutS/B_{12}-nucleotide loop complex. For example, the proximity of the aromatic dimethylbenzimidazole in the B_{12}-nucleotide loop to the central β-sheet (β3 and β4, Figures 7A and 7B) was indicated by intermolecular NOEs between C10/C11, cf. Figure 6A, and the amide protons $^{1}H^{N}$ of S62 (β3) and V90 and G91 (β4) (Tollinger et al., 2001). Additional intermolecular NOEs (between the protons C10/C11 and the $^{1}H^{N}$'s of I6, V60, Y117 and T126) further corroborated an analogous binding mode of the nucleotide in MutS, compared to the holoenzyme crystal structure of glutamate mutase (Reitzer et al., 1999). Interestingly, however, several NOEs could not be detected for ^{15}N-labeled MutS that would be expected based on the X-ray structure of glutamate mutase reconstituted with methylcobalamin (Reitzer et al., 1999) (e.g., H(C10/C11)-$^{1}H^{N}$(G9,C59); H(C4)-$^{1}H^{N}$(V60,S61). Likewise, no intermolecular NOEs could be assigned for protons of the ribose ring or isopropanolamin unit of the B_{12}-nucleotide. This indicated, together with the observed chemical shifts, a time averaged position of the B_{12}-nucleotide somewhat more towards the entrance of the binding pocket (Tollinger et al., 2001). The enlarged number of unambiguously assigned intermolecular NOEs obtained with the sequence of Figure 1, in particular NOE connectivities between protons of the ribose R5 and the methyl group Pr3 of the isopropanolamin unit and protons of MutS allow now a better characterization of the binding site.

It is also important to note, that due to the high molar concentration (≈24 mM) of the unlabeled B_{12}-nucleotide loop, intramolecular B_{12}-nucleotide NOE

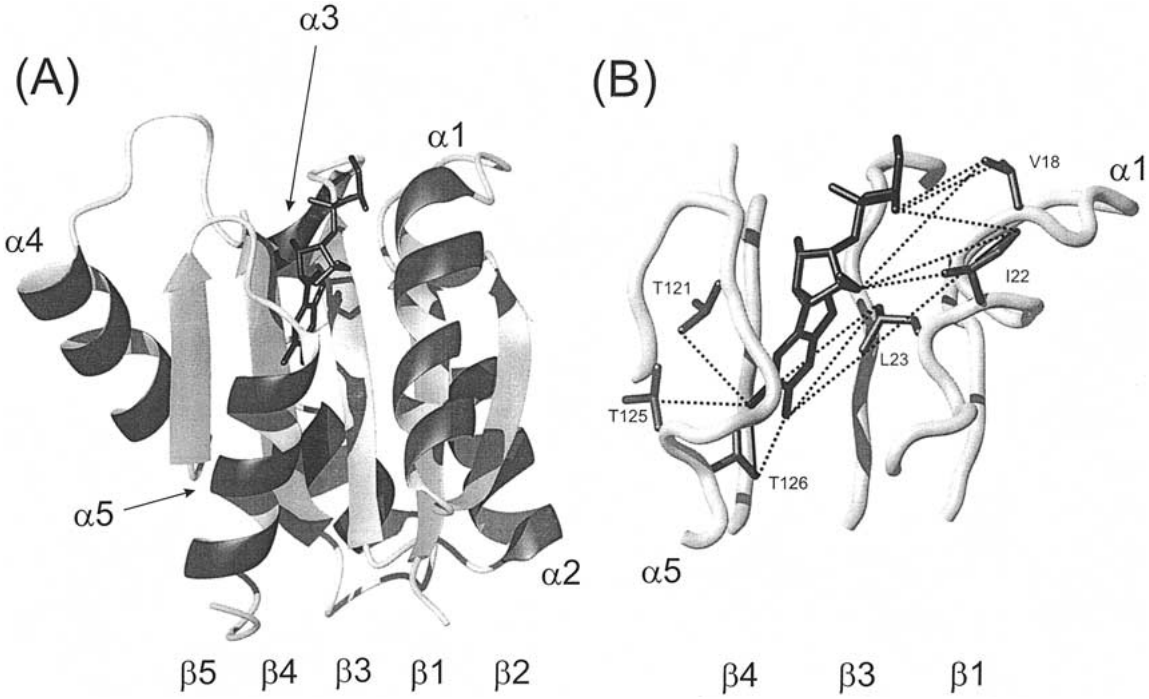

Figure 7. Ribbon diagramm showing the B_{12}-nucleotide binding cleft of MutS. (A) Structural homology model for the B_{12}-nucleotide binding site in MutS (based on the crystal structure of glutamate mutase from *Clostridium cochlearium*, Reitzer et al., 1999). The location of the B_{12}-nucleotide binding site in MutS was obtained from the closely related complex between glutamate mutase from *Clostridium cochlearium* and methylcobalamin (see text) (Reitzer et al., 1999) and independently confirmed in solution by ^{15}N chemical shift perturbation (Tollinger et al., 2001). Secondary structure elements are numbered. Only the nucleotide moiety of bound methylcobalamin is shown. (B) Schematic diagram showing the helices α1 and α5 and β-strands β1, β3 and β4 of MutS and the intermolecular MutS/ B_{12}-nucleotide NOEs observed with the sequence of Figure 3 (dashed lines). The figure was prepared using the program MOLMOL (Koradi et al., 1996).

cross peaks at natural abundance become visible in the intermolecular NOE data set (see Figure 6B). For example, in the lower panel of Figure 6B, the cross peak denoted by ** is due to an intramolecular NOE between the degenerate methyl groups C10 and C11 of the dimethylbenzimidazole moiety. However, these intramolecular cross peaks can also be used for structural refinement purposes (e.g., to better characterize the geometry of the bound ligand). Specifically, we observed the following intramolecular dipolar connectivities: C7-R1, C7-C11, R5-R4, Pr2-Pr3, and Pr1-Pr3, which will be beneficial for the refinement of the protein bound conformation (e.g., sugar pucker, glycosidic angle) of the B_{12}-nucleotide loop.

Conclusions

A novel method for simultaneous recording of inter- and intramolecular NOEs in molecular complexes consisting of ^{15}N,^{13}C-labeled proteins and unlabeled ligands has been presented. The method relies on a selective inversion of protein protons (attached to ^{13}C and ^{15}N) by applying an adiabatic ^{13}C frequency sweep optimized for the empirically observed relationship between the heteronuclear one-bond scalar coupling constant $^{1}J_{CH}$ and the ^{13}C chemical shift. Two data sets are recorded in which the relative signs of ligand and protein Zeeman magnetizations during the NOESY mixing period are inverted. Addition or subtraction of the two data sets results in pure intramolecular or intermolecular NOESY maps, respectively. The particular merits of the proposed filtering method is the significant $^{1}J_{CH}$-bandwidth and a substantial time saving by allowing the simultaneous measurement of intra- and intermolecular NOEs. Data obtained on the low-affinity complex between the B_{12}-binding subunit of glutamate mutase from *Clostridium tetanomorphum* and the B_{12}-nucleotide loop also suggest possible applications to studies of macromolecular complexes in the context of SAR by NMR (Shuker et al., 1996).

Acknowledgements

The authors thank Prof N.E.G. Marsh (University of Ann Arbor) for kindly supplying uniformly ^{13}C,^{15}N-labeled MutS, and Mag. Wolfgang Fieber for fruitful discussions. This research was supported by grants P 13595 (to B.K.) and P 13486 (to R.K.) from the Austrian Science Foundation FWF, and the European Commission (TMR Project No. FMRX.CT96.0018, to B.K.).

References

Bartels, G., Nussberger, R., Kreppelt, F. and Eschenmoser, A., unpublished, see Kreppelt, F. (1991) Thesis, ETH-Zürich, No. 9458.

Bax, A., Grzesiek, S., Gronenborn, A.M. and Clore, G.M. (1994) *J. Magn. Reson. Ser.*, **A106**, 269–273.

Böhlen, J.M. and Bodenhausen, G. (1993) *J. Magn. Reson. Ser.*, **A102**, 293.

Breeze, A. (2000) *Prog. NMR Spectr.*, **36**, 323–372.

Clore, G.M. (2000) *Proc. Natl. Acad. Sci. USA*, **97**, 9021–9025.

Clore, G.M. and Gronenborn, A.M. (1997) *Nat. Struct. Biol.*, **4**, Suppl S, 849–853.

Dalvit, C., Cottens, S., Ramage, P. and Hommel, U. (1999) *J. Biomol. NMR*, **13**, 43–50.

Dalvit, C., Ramage, P. and Hommel, U. (1998) *J. Magn. Reson.* **131**, 148–153.

Delaglio, F., Grzesiek, S., Vuister, G.W., Zhu, G., Pfeifer, J. and Bax, A. (1995) *J. Biomol. NMR*, **6**, 277–293.

Drennan, C.L., Huang, S., Drummond, J.T., Matthews, R.G. and Ludwig, M.L. (1994a) *Science*, **266**, 1669–1674.

Drennan, C.L., Matthews, R.G. and Ludwig, M.L. (1994b) *Curr. Opin. Struct. Biol.*, **4**, 919–929.

Eschenmoser, A. (1988) *Angew. Chem. Int. Ed. Engl.* **100**, 5–40.

Folkers, P.J.M., Folmer, R.H.A., Konings, R.N.H. and Hilbers, C.W. (1993) *J. Am. Chem. Soc.*, **115**, 3798–3799.

Folkers, P.J.M., Nilges, M., Folmer, R.H.A., Konings, R.N.H. and Hilbers, C.W. (1994) *J. Mol. Biol.*, **236**, 229–246.

Geen, H. and Freeman, R. (1991) *J. Magn. Reson.*, **93**, 93–141.

Gemmecker, G., Olejniczak, E.T. and Fesik, S.W. (1992) *J. Magn. Reson.*, **96**, 199–204.

Hoffmann, B., Konrat, R., Tollinger, M., Huhta, M.S., Marsh, E.N.G., and Kräutler, B. (2001) *Chem. Bio. Chem.*, in press.

Ikura, M. and Bax, A. (1992) *J. Am. Chem. Soc.*, **114**, 2433–2440.

Johnson, B.A. and Blevins, R.A. (1994) *J. Biomol. NMR*, **4**, 603–614.

Koradi, R., Billeter, M. and Wüthrich, K. (1996) *J. Mol. Graphics*, **14**, 51–55.

Kupce, E. and Freeman, R. (1995) *J. Magn. Reson. Ser.*, **A115**, 273–276.

Lee, W., Revington, M.J., Arrowsmith, C. and Kay, L.E. (1994) *FEBS Lett.*, **350**, 87–90.

Mancia, F., Keep, N.H., Nakagawa, A., Leadlay, P.F., McSweeney, S., Rasmussen, B., Bösecke, P., Diat, O. and Evans, P.R. (1996) *Structure*, **4**, 339–350.

Marion, D., Ikura, M., Tschudin, R. and Bax, A. (1989) *J. Magn. Reson.*, **85**, 393–399.

McCoy, M. and Mueller, L. (1992) *J. Am. Chem. Soc.*, **114**, 2108–2112.

Melacini, G. (2000) *J. Am. Chem. Soc.*, **122**, 9735–9738.

Otting, G. and Wüthrich, K. (1990) *Quart. Rev. Biophys.*, **23**, 39–96.

Otting, G., Senn, H., Wagner, G. and Wüthrich, K. (1986) *J. Magn. Reson.*, **85**, 500–505.

Pascal, S.M, Muhandiram, D.R., Yamazaki, T., Forman-Kay, J.D. and Kay, L.E. (1994) *J. Magn. Reson. Ser.*, **B103**, 197–201.

Reitzer, R., Gruber, K., Jogl, G., Wagner, U.G., Bothe, H., Buckel, W. and Kratky, C. (1999) *Structure*, **7**, 891–902.

Sattler, M., Schleucher, J. and Griesinger, C. (1999) *Prog. NMR Spectr.*, **34**, 93–158.

Shaka, A.J., Barker, P.B. and Freeman, R. (1985) *J. Magn. Reson.*, **64**, 547–552.

Shaka, A.J., Keeler, J., Frenkiel, T. and Freeman, R. (1983) *J. Magn. Reson.*, **52**, 335–338.

Shuker, S.B., Hajduk, P.J., Meadows, R.P. and Fesik, S.W. (1996) *Science*, **274**, 1531–1534.

Stuart, A.C., Borzilleri, K.A., Withka, J.M. and Palmer, III, A.G., (1999) *J. Am. Chem. Soc.*, **121**, 5346–5347.

Tollinger, M., Konrat, R., Eichmüller, C., Huhta, M.S., Marsh, E.N.G. and Kräutler, B. (2001) *J. Mol. Biol.*, in press.

Tollinger, M., Konrat, R., Hilbert, B.N., Marsh, E.N.G. and Kräutler, B. (1998) *Structure*, **6**, 1021–1033.

Wider, G., Weber, C., Traber, H., Widmer, H. and Wüthrich, K. (1990) *J. Am. Chem. Soc.*, **112**, 9015–9016.

Wider, G., Weber, C. and Wüthrich, K. (1991) *J. Am. Chem. Soc.*, **113**, 4676–4678.

Wörgötter, E., Wagner, G. and Wüthrich, K. (1986) *J. Am. Chem. Soc.*, **108**, 6162.

Yang, J.C., Ramesh, V. and Roberts, G.C.K. (1995) *J. Magn. Reson. Ser.*, **B106**, 284.

Zwahlen, C., Legault, P., Vincent, S.J.F., Greenblatt, J., Konrat, R. and Kay, L.E. (1997) *J. Am. Chem. Soc.*, **119**, 6711–6721.

Zwahlen, C., Vincent, S.J.F., Di Bari, L., Levitt, M.H. and Bodenhausen, G. (1994) *J. Am. Chem. Soc.*, **116**, 362–368.